Computer Life (CPL) ISSN: 1819-4818
DELIVERING QUALITY SCIENCE TO THE WORLD

Frequency domain design method of wavelet basis based on pulsar signal

Pengfei Zhang [a], Hongli Wang and Yuxuan Zhang

Department of Missile Engineering, Rocket Force University of Engineering, Xi'an, Shaanxi 710025, China

[a] zpfei1215@163.com

Abstract: In order to improve the wavelet denoising effect of pulsar signal, a wavelet basis designed method by frequency analysis is proposed. Firstly, the pulsar signal is analyzed in the frequency domain. According to its frequency domain characteristics, the wavelet basis CPn (Crab Pulsar wavelet basis, n is the length of the wavelet basis) is designed, and then the lifting algorithm is implemented. The simulation results show that CPn has better noise reduction effect, the signal noise ratio can be improved by 4dB, the mean square error is reduced by 61%, and the peak relative error is reduced by 45%.
Keywords: pulsar navigation; wavelet basis; lifting wavelet; frequency domain analysis; denoising.

1. INTRODUCTION

A pulsar is a high-speed rotating neutron star that radiates electromagnetic waves of various wavelengths to the periodic surroundings. The navigation method that uses one or more pulsars as a signal source is called pulsar navigation. As a new type of autonomous navigation, it has attracted wide attention from scholars all around the world (Yu, Xu, Feng, He, & Ye, 2015)(Xu, Wang, Feng, Jiang, et al., 2018)(Xu, Wang, Feng, You, & He, 2018)(You et al., 2018). Pulsar navigation uses the pulsar's periodic electromagnetic waves as the signal source to obtain the position and time information by calculating the phase of the signal. There are three problems in the process of signal processing. First, because the universe contains a lot of background noise, and the signal detector itself contains noise caused by dark current, etc., the obtained pulse contour contains a lot of noise. Second, the signal of the distant pulsar reaching the detector is very weak and has been attenuated into the form of a single photon. Third, because the effective area of the detector is small, it takes a long time to accumulate. These three problems affect the accuracy of the TOA estimate, thereby reducing the accuracy of positioning and punctuality. So the pulsar signal must be denoised.

The noise reduction method based on wavelet transform has been applied in many fields (Wei, Yue, Wei, Haiyu, & Ya, 2012) (Liu, He, Guo, & Tang, 2016). In (Xiao-ming, Fu-cheng, & Yuan-yan, 2006), wavelet transform was applied to the denoising of pulsar signal for the first time, and the selection of wavelet basis and the number of decomposition layers were studied. This document proved that the wavelet transform could greatly improve the signal-to-noise ratio, and the

high-frequency information of the useful signal was not lost. Literature (Li, Xi-zheng, & Guang-ren, 2008) studied the selection of the optimal threshold, and selected Coiflets as the wavelet basis for analyzing the pulse signal from wo angles of tight support and vanishing distance. However, the processing of the threshold does not solve the contradiction between suppressing noise and retaining details. Literature (Di, Xu, & Zhenhua, 2007) introduces fuzzy theory into the threshold processing algorithm of wavelet denoising. A membership function was established to distinguish between signals and noise, and noise was suppressed while preserving the signal. In (Zhe, Xu, Yo, Zhen, & Nan, 2010), an improved wavelet spatial correlation filter denoising method was proposed, which could further improve the ability to preserve signals while suppressing noise. Literature (Xue et al., 2016) proposed a local linear minimum mean square error method for unsampled wavelet domain, which could continue to improve both signal-to-noise ratio and signal retention.

The above scholars mainly focused on the selection of wavelet basis and the design of wavelet threshold function. The choice of wavelet basis is the base of wavelet denoising, so if the wavelet basis selection is inappropriate, it will directly affect the denoising effect. There is currently no universal wavelet basis that accommodates all signals, so the most appropriate wavelet basis for different signals is different. The above mentioned literatures usually used existing wavelet basis for the selection of wavelet basis, and did not design special wavelet basis for pulsar signals. Few literatures have studied the design of wavelet basis for pulsar signals. The wavelet basis set CPn (Crab Pulsar wavelet basis, n represents the wavelet basis length) for the pulsar signal is designed. This set of wavelet basis can make the denoised signal get higher signal to noise ratio, lower mean square error and peak position error.

The rest of the article is organized as follows. In Section 2, the signal of the Crab pulsar is analyzed by the frequency domain method, and then the wavelet basis is designed. Section 3 implements a wavelet lifting algorithm. The simulation is carried out in Section 4 and the simulation results are analyzed. Section 5 gives the conclusion.

2. FREQUENCY DOMAIN ANALYSIS OF PULSAR SIGNAL AND CONSTRUCTION OF WAVELET BASIS

2.1 Analysis of frequency characteristics of pulsar signal

The literature (Fang et al., 2016) proves that the TOA estimation can completely abandon the high-frequency part information that is greatly interfered by noise, and only uses the low-frequency part information with high signal-to-noise ratio. The FFT (fast fourier transformation) is performed on the actual profile of the Crab pulsar data of the actual period of 1 s and the actual noisy profile obtained by epoch folding, as shown in Fig. 1. By comparing the FFT amplitude-frequency curves, it can be seen that the ideal curve mainly concentrates on the low frequency near 0 Hz, and the noise-containing curve has components in the range of 20-40 Hz. When designing low-pass filters, the cut-off frequency should be as close as possible to 0 Hz, and the curve of the filters should be as vertical as possible to the X-axis, so as to approach the ideal filter. The closer to the ideal filter, the higher the order of the filter is required, but the higher the order, the larger the amount of calculation. Therefore, when designing the wavelet basis, the contradiction between the calculation amount (order) and the signal-to-noise ratio should be balanced.

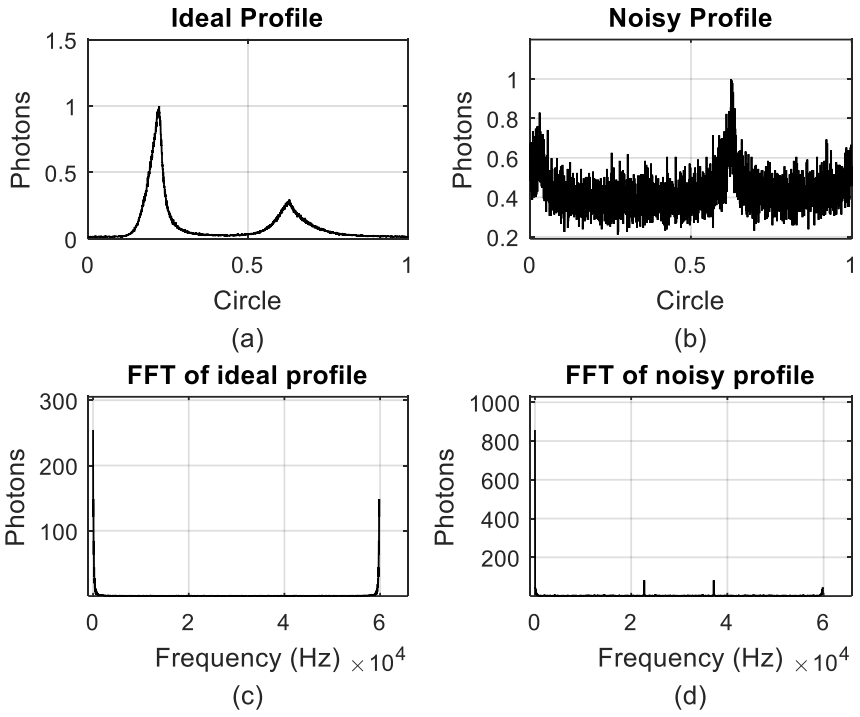

Fig. 1 Waveform and FFT Transform of Ideal profile and Noisy profile

2.2 Construction of Wavelet Basis

Constructing a wavelet basis requires two principles of linear phase and convergence. The reason is as follows. If phase distortion will affect the TOA estimation of subsequent pulsar signals, thus affecting the positioning and punctuality of pulsar navigation, the process of pulsar signal denoising cannot be phase-distorted. First, phase distortion affects the TOA estimation of subsequent pulsar signals, which affects the positioning and punctuality of pulsar navigation. Therefore, the process of pulsar signal denoising cannot be phase-distorted. Secondly, if the filtered curve diverges, the filtering purpose cannot be achieved, and the waveform will also be deformed, so it is desirable that the filtered curve converges.

The CPn wavelet basis cluster is designed by the hamming window method, which is compared with the Dbn wavelet basis cluster as shown in Fig. 2. Subgraphs (a)-(d) correspond to Dbn and CPn of lengths 4, 6, 8, and 10. It can be seen from the figure that the coefficients of CPn follow the even or odd symmetry. Therefore, the phase delay and group delay of CPn are equal and constant in the frequency band. For CPn of n-order linear phase, the group delay is $n/2$. That is to say, the signal after wavelet transform is simply delayed by $n/2$ steps. This attribute preserves the waveform of the signal in the passband, that is, there is no phase distortion.

The FFT of wavelet basis of lengths 4, 6, 8, and 10 corresponds to (a)-(d) subgraphs of Fig. 3, respectively. In the case of the same length, all CPn wavelet-basis low-pass filter amplitude-frequency curve hCPn and high-pass filter amplitude-frequency curve gCPn are respectively below Dbn's low-pass filter amplitude-frequency curve hDbn and high-pass filter amplitude-frequency curve gDbn. That is to say, the angle between the curve and the Y axis is smaller. So closer to the ideal filter, in theory, the filtering effect is better.

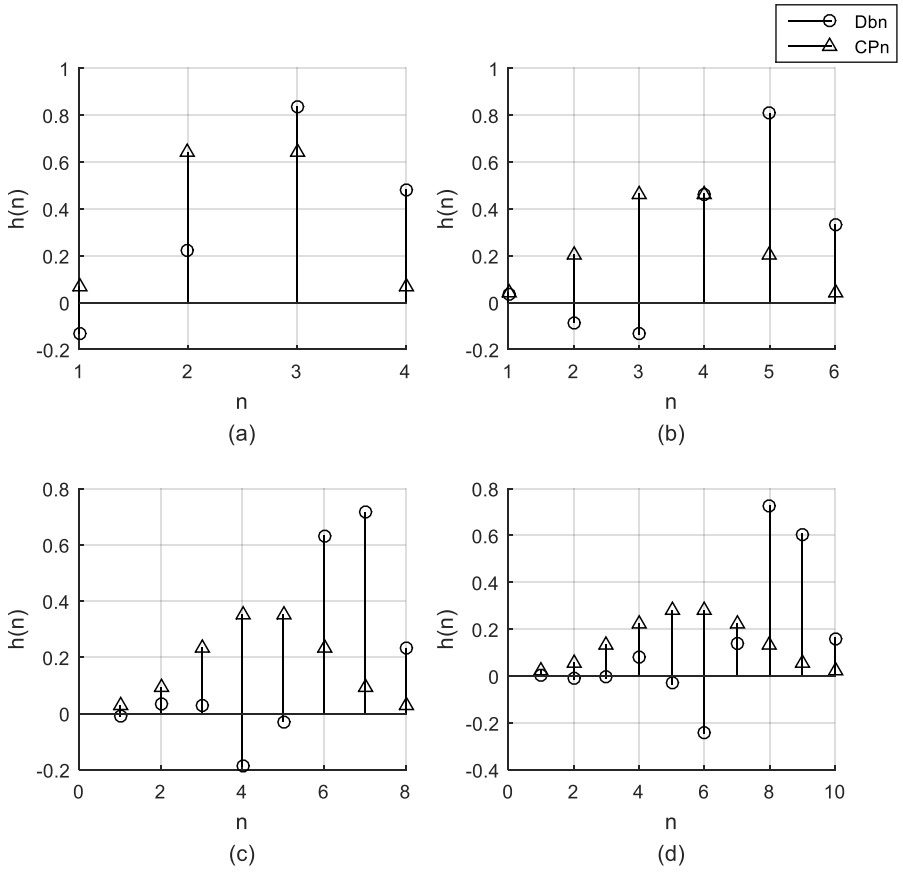

Fig. 2 Comparisons of Dbn and CPn wavelet basis with different lengths

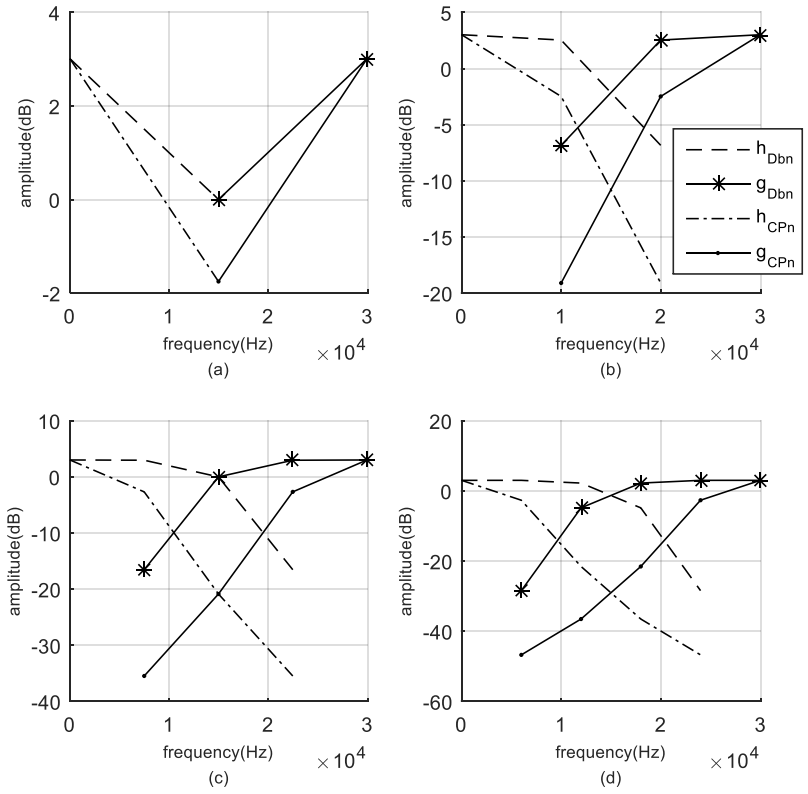

Fig. 3 Comparison of FFT Transform of Dbn and CPn Wavelet Basis with Different Length

The pole-zero diagrams of CPn of lengths 4, 6, 8 and 10 correspond to the sub-graphs (a)-(d) of Fig. 4.

It can be seen from the figure that the poles of CPn are all within the unit circle, so they are stable and will not diverge after wavelet transformation.

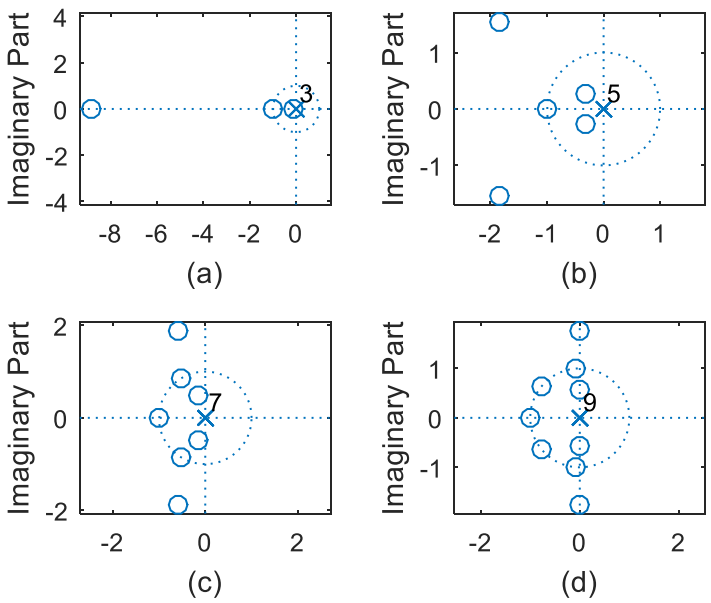

Fig. 4 Zero-Pole Maps of CPn wavelet basis with different length

3. IMPLEMENTATION OF LIFTING ALGORITHM

The lifting algorithm is a more flexible and more versatile tool than the traditional wavelet, which is independent of the Fourier transform (Sweldens, 1998). Because the lifting algorithm first downsamples and then convolutions, it can reduce the complexity of the algorithm by half compared to traditional wavelets. The process of lifting the algorithm is mainly divided into three steps, as shown in Fig. 5.

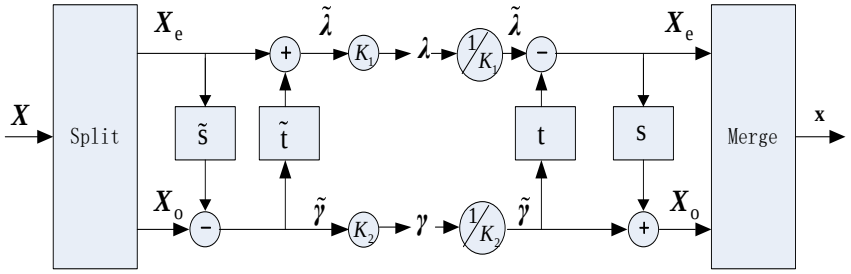

Fig. 5 Basic flow of lifting algorithms

First step, split

The pulsar profile signal X after epoch folding is divided into odd and even two sets of two vectors X_e and X_o which do not intersect each other according to the index value i.

Second step, prediction

Designing the prediction operator $\tilde{s}$, combining X_e and X_o to obtain the prediction bias $\tilde{\gamma}$, can be considered as the high frequency coefficient of X.

Third step, update

Designing the update operator $\tilde{t}$, combining $\tilde{\gamma}$ and X_e, yields the approximation coefficient $\tilde{\lambda}$.

The above 3 steps are only ideal, but the actual situation may be more complicated. In fact, there may be multiple predictions and updates, and there may be multiple scale-ups, such as K_1 and K_2 in Fig. 5. The process of implementing the lifting algorithm for $\mathrm{h_{CPn}}$ and $\mathrm{g_{CPn}}$ is as follows.

According to

$$\begin{aligned}\lambda(z) &= \tilde{\mathrm{h}}_{\mathrm{CPn}}(z)\boldsymbol{X}(z) \\ &= \tilde{\mathrm{h}}_{\mathrm{e}}(z)\boldsymbol{X}_e(z) + z^{-1}\tilde{\mathrm{h}}_{\mathrm{o}}(z)\boldsymbol{X}_o(z)\end{aligned} \tag{1}$$

and

$$\begin{aligned}\gamma(z) &= \tilde{\mathrm{g}}_{\mathrm{CPn}}(z)\boldsymbol{X}(z) \\ &= \tilde{\mathrm{g}}_{e}(z)\boldsymbol{X}_e(z) + z^{-1}\tilde{\mathrm{g}}_{o}(z)\boldsymbol{X}_o(z)\end{aligned}, \tag{2}$$

a matrix form equation

$$\begin{bmatrix}\boldsymbol{\lambda}\\ \boldsymbol{\gamma}\end{bmatrix} = \begin{bmatrix}\tilde{\mathrm{h}}_{\mathrm{e}}(z) & \tilde{\mathrm{h}}_{\mathrm{o}}(z)\\ \tilde{\mathrm{g}}_{\mathrm{e}}(z) & \tilde{\mathrm{g}}_{\mathrm{o}}(z)\end{bmatrix}\begin{bmatrix}\boldsymbol{X}_{\mathrm{e}}(z)\\ z^{-1}\boldsymbol{X}_{\mathrm{o}}(z)\end{bmatrix} \tag{3}$$

is obtained. A multiphase matrix

$$\tilde{\boldsymbol{P}} = \begin{bmatrix}\tilde{\mathrm{h}}_{\mathrm{e}}(z) & \tilde{\mathrm{h}}_{\mathrm{o}}(z)\\ \tilde{\mathrm{g}}_{\mathrm{e}}(z) & \tilde{\mathrm{g}}_{\mathrm{o}}(z)\end{bmatrix} \tag{4}$$

can be obtained. According to

$$\boldsymbol{P}(z) = \begin{pmatrix}\tilde{\mathrm{h}}_{\mathrm{e}}(z) & \tilde{\mathrm{h}}_{\mathrm{o}}(z)\\ \tilde{\mathrm{h}}_{\mathrm{e}}(z)\mathrm{t}(z) + \tilde{\mathrm{g}}_{\mathrm{e}}^{\mathrm{new}}(z) & \tilde{\mathrm{h}}_{\mathrm{o}}(z)\mathrm{t}(z) + \tilde{\mathrm{g}}_{\mathrm{o}}^{\mathrm{new}}(z)\end{pmatrix} = \begin{pmatrix}1 & 0\\ \tilde{\mathrm{t}}(z) & 1\end{pmatrix}\boldsymbol{P}^{new}(z) \tag{5}$$

and

$$\tilde{\boldsymbol{P}}(z) = \begin{pmatrix}\tilde{\mathrm{h}}_{\mathrm{e}}(z) + \tilde{\mathrm{g}}_{\mathrm{e}}(z)\tilde{\mathrm{s}}(z) & \tilde{\mathrm{h}}_{\mathrm{o}}(z) + \tilde{\mathrm{g}}_{\mathrm{o}}(z)\tilde{\mathrm{s}}(z)\\ \tilde{\mathrm{g}}_{\mathrm{e}}(z) & \tilde{\mathrm{g}}_{\mathrm{o}}(z)\end{pmatrix} = \begin{pmatrix}1 & \tilde{\mathrm{s}}(z)\\ 0 & 1\end{pmatrix}\tilde{\boldsymbol{P}}^{new}(z)\ , \tag{6}$$

$\tilde{\boldsymbol{P}}(z)$ can be converted into a lifted form

$$\mathbf{P}(z) = \prod_{i=1}^{m}\left\{\begin{pmatrix}1 & \mathrm{s}_i(z)\\ 0 & 1\end{pmatrix}\begin{pmatrix}1 & 0\\ \mathrm{t}_i(z) & 1\end{pmatrix}\right\}\cdot\begin{pmatrix}K_1 & 0\\ 0 & K_2\end{pmatrix}. \tag{7}$$

Its analytic formula is

$$\mathbf{P}(z) = \begin{bmatrix}1 & 1\\ 0 & 1\end{bmatrix}\begin{bmatrix}1 & 0\\ -\frac{1}{2} & 1\end{bmatrix}\begin{bmatrix}2K_1 & 0\\ 0 & K_2\end{bmatrix}. \tag{8}$$

So the prediction operator is

$$t(z) = -\frac{1}{2}\ , \tag{9}$$

and the update operator is

$$s(z) = 1 \tag{10}$$

K_1 and K_2 are shown in the Table 1.

Table 1 K1 and K2 in Analytic Formula of CPn Lifting Algorithms

Wavelet basis	$\boldsymbol{K_1}$	$\boldsymbol{K_2}$
CP4	$(4.56E-02)\cdot Z+(4.54E-01)\cdot Z^2$	$(4.56E-02)+(4.54E-01)\cdot Z$
CP6	$(2.64E-02)+(3.33E-01)\cdot Z$ $+(1.40E-1)\cdot Z^2$	$(2.64E-02)+(3.33E-01)\cdot Z$ $+(1.40E-1)\cdot Z^2$

CP8	$(1.74E-02)\cdot Z+(1.66E-01)\cdot Z^2$ $+(2.55E-01)\cdot Z^3+(6.12E-02)\cdot Z^4$	$(1.74E-02)+(1.66E-01)\cdot Z$ $+(2.55E-01)\cdot Z^2+(6.12E-02)\cdot Z^3$
CP10	$(1.19E-02)Z+(8.88E-02)\cdot Z^2$ $+(2.07E-01)\cdot Z^3+(1.59E-01)\cdot Z^4$ $+(3.25E-02)\cdot Z^5$	$(1.19E-02)+(8.88E-02)\cdot Z$ $+(2.07E-01)\cdot Z^2+(1.59E-01)\cdot Z^3$ $+(3.25E-02)\cdot Z^4$

4. SIMULATION AND DISCUSSION

The numerical simulation hardware and software parameters are shown in Table 2.

Table 2 Simulation parameter

Name	Parameters
Pulsar data sources	RXTE data from NASA.(The experimental results are in Section 4.) XPNAV-1 and HXMT (See the appendix for the experimental results.)
Wavelet basis	lowpass FIR digital filter of Hamming window
Length of Wavelet basis	4, 6, 8 and 10
Computer	Win7 X64,:i5-3210M, 2.5GHz, 16GB RAM
Matlab	R2015a

To verify the validity of the proposed method, two sets of Dbn and CPn wavelet basis of the same length were compared. The indicators for evaluation are as follows.

SNR (signal to noise ratio)

$$SNR = 10 \cdot \lg\left[\frac{\sum_{i=1}^{N} \boldsymbol{y}^2}{\sum_{i=1}^{N} (\boldsymbol{y} - \hat{\boldsymbol{y}})^2}\right] \tag{11}$$

where y is the original signal, $\hat{y}$ is the denoised signal, and N is the signal length.

MSE (mean square error)

$$MSE = \frac{\sum_{i=1}^{N} (\mathbf{y} - \hat{\mathbf{y}})^2}{N} \tag{12}$$

PRE (Peak relative error)

$$PRE = \frac{|V_0 - V_d|}{V_0} \cdot 100\% \tag{13}$$

where V_0 is the pulse peak of the standard pulse profile and V_d is the peak of the pulsar signal after denoising. The filtering effect of different length filters is shown in Fig. 6. For clarity, the filtered curve is moved vertically. It can be seen that the CPn wavelet-basis filtered curve is smoother and closer to the ideal curve, so its filtering effect is better.

CC(correlation coefficient)

$$CC = \frac{\mathrm{cov}(\mathrm{y}, \hat{\mathrm{y}})}{\sqrt{\mathrm{var}(\mathrm{y})\,\mathrm{var}(\hat{\mathrm{y}})}} \tag{14}$$

where $\mathrm{cov}(\mathrm{y}, \hat{\mathrm{y}})$ is the covariance of y and $\hat{\mathrm{y}}$, and $\mathrm{var}(\mathrm{y})$ and $\mathrm{var}(\hat{\mathrm{y}})$ are the variances of y and $\hat{\mathrm{y}}$, respectively.

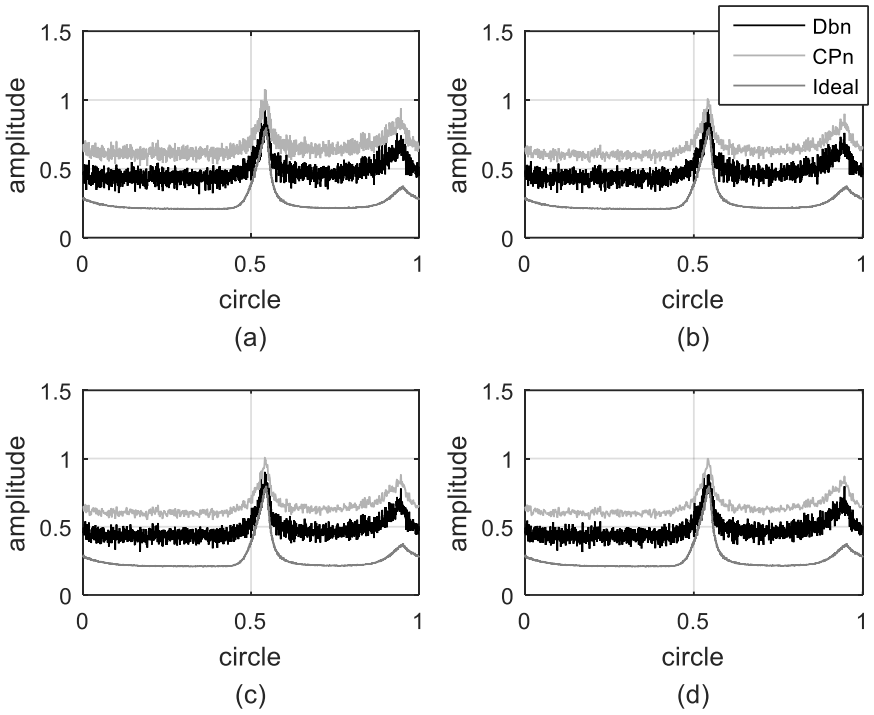

Fig. 6 Denoising effect of CPn and DBn of different lengths (RXTE data)

The denoising effects of the two wavelet basis of Dbn and CPn are shown in Table 2 and Table 3. It can be seen from the two tables that the SNR of CPn is higher than the SNR of Dbn in the same length, and even the CP4 wavelet basis of length 4 is higher than the SNR of DB5 wavelet basis of length 10. CPn's MSE and PRE indicators are also better than that of Dbn. In the case of level 1 decomposition, the SNR of the wavelet basis length is 10, and the MSE and the PRE reach the highest at the same time. Compared with Db5, CP10 has 4dB higher SNR, 61% lower MSE and 45% lower PRE. On the whole, both the CPn wavelet basis and the Dbn wavelet basis conform to the law that the noise reduction effect is better with the increase of the wavelet basis length.

However, as the length increases, it will inevitably lead to an increase in the calculation, which increases the calculation time and takes up more hardware resources. If on a platform with parallel computing, filters of different lengths can be calculated simultaneously, this can parallelize the complex filtering process, which can greatly reduce the calculation time. Then the optimal filter is selected by the cost function to realize adaptive wavelet basis selection. Compared with the Dbn wavelet basis, the CPn wavelet basis not only has a good filtering effect, but the algorithm is not more complicated. When the length of the analyzed data is fixed and the threshold collapse algorithm is determined, the complexity of the wavelet denoising algorithm is only related to the length of the wavelet basis. So when the CPn wavelet basis and the Dbn wavelet basis are the same length, their algorithm complexity is the same. That is, the time consumption of the algorithm is basically the same.

Table 3 1-Level filtering effect of different wavelet basis (RXTE data)

Wavelet basis	SNR (dB)	MSE	PRE	CC
DB2	6.53e+00	5.35e-02	1.56e-01	7.98e-01
CP4	6.55e+00	5.32e-02	1.23e-01	8.21 e-01
DB3	6.54e+00	5.35e-02	1.67e-01	8.02 e-01

CP6	6.59e+00	5.27e-02	5.12e-02	8.57 e-01
DB4	6.54e+00	5.35e-02	1.27e-01	8.02 e-01
CP8	6.59e+00	5.26e-02	4.93e-02	8.66 e-01
DB5	6.53e+00	5.35e-02	1.06e-01	8.01 e-01
CP10	6.60e+00	5.25e-02	4.30e-02	8.71 e-01

Table 4 2-Level filtering effect of different wavelet basis (RXTE data)

Wavelet basis	SNR (dB)	MSE	PRE	CC
DB2	6.57e+00	5.29e-02	6.90e-02	8.43e-01
CP4	6.59e+00	5.27e-02	6.72e-02	8.59e-01
DB3	6.58e+00	5.29e-02	5.99e-02	8.45e-01
CP6	6.60e+00	5.24e-02	3.67e-02	8.77e-01
DB4	6.58e+00	5.28e-02	9.65e-02	8.45e-01
CP8	6.60e+00	5.24e-02	2.82e-02	8.81e-01
DB5	6.58e+00	5.28e-02	5.80e-02	8.46e-01
CP10	6.61e+00	5.24e-02	2.10e-02	8.83e-01

5. CONCLUSION

This paper designs a set of wavelet basis CPn basisd on frequency analysis and implements its lifting algorithm. Compared with the traditional Dbn wavelet basis cluster, there are improvements in SNR, MSE and PRE. Compared with the traditional Dbn wavelet basis cluster, there are improvements in SNR, MSE and PRE. The set of wavelet basis can select a wavelet basis of a suitable length according to different requirements of accuracy and calculation amount. The design method of this wavelet base is not only suitable for Crab pulsar signal, but also can be applied to other pulsar signal denoising. The method can provide a signal source with higher signal-to-noise ratio for the TOA estimation algorithm, thereby more accurately estimating the TOA, and finally improving the accuracy of the pulsar navigation.

REFERENCES

[1] D. Yan, L.P. Xu, Z.H. Xie: Wavelet Denoising Algorithm Based on Fuzzy Threshold f or Pulsar Signal, Journal of Xi'an Jiaotong University, Vol. 41 (2007) No.10, p.1193-1196.
[2] H.Y. Fang, B. L, X.P. L, et al: Time delay estimation method of X-ray pulsar observed profile based on the optimal frequency band, Acta Physica Sinica, Vol. 65 (2016) No.11, p.317-325.
[3] L. Wang, X.Z. Ke, G.R. Ni: Research on Noise Reduction for Millisecond Pulsar Signal Based on Wavelet Transform, ASTRONOMICAL RESEARCH &TECHNOLOGY, Vol. 5 (2008) No.1, p.49-54.
[4] Z. Liu, Z. He, W. Guo, Z. Tang: A hybrid fault diagnosis method based on second generation wavelet de-noising and local mean decomposition for rotating machinery, ISA Transactions, Vol. 61 (2016) No.1, p.211-220.
[5] W. I. M. Sweldens: THE LIFTING SCHEME: A CONSTRUCTION OF SECOND GENERATION WAVELETS, SIAM Journal on Mathematical Analysis, Vol. 29 (1998) No.2, p.511-546.
[6] G. Wei, Z. Yue, Z. Ya: Research on real-time de-noising of FOG based on second generation wavelet transform, Chinese Journal of Scientific Instrument, Vol. 33 (2012) No.4, p.774-780.
[7] Z. Xiao-ming, L. Fu, T. Yuan: Pulsar Signal Denoising Based on Wavelet Transformation, ACTA ASTRONOMICA SINICA, Vol. 47 (2006) No.3, p.238-335.
[8] Q. Xu, H. Wang, L. Feng, S. You: A novel X-ray pulsar integrated navigation method for ballistic aircraft, Optik, Vol. 175 (2018) No.5, p.28-38.
[9] Q. Xu, H. Wang, L. Feng, W. Jiang: An improved augmented X-ray pulsar navigation algorithm based on the norm of pulsar direction error, Advances in Space Research, Vol. 62 (2018) No.11, p.3187-3198.

[10] M. Xue, X. Li, H. Sun: Denoising of X-ray pulsar observed profile in the undecimated wavelet domain, Acta Astronautica, Vol. 118 (2016) No.1, p.1-10.
[11] S. You, H. Wang, Y. He, Q. Xu, J. Lu, L. Feng: Pulsar Profile construction based on Double-Redundant-Dictionary and Same-Scale L1-Norm Compressed Sensing, Optik, Vol. 164 (2018) No.25, p.617-623.
[12] H. Yu, L. Xu, D. Feng, X. He, X. Ye: A sparse representation-based optimization algorithm for measuring the time delay of pulsar integrated pulse profile, Aerospace Science and Technology, Vol. 46 (2015) No.25, p.94-103.